mathematics

MDPI

Article

High-Efficiency e-Powertrain Topology by Integrating Open-End Winding and Winding Changeover for Improving Fuel Economy of Electric Vehicles

Kyoung-Soo Cha [1,†], Jae-Hyun Kim [2,†], Sung-Woo Hwang [3], Myung-Seop Lim [3,*] and Soo-Hwan Park [4,*]

[1] Advanced Mobility System Group, Korea Institute of Industrial Technology, Daegu 42994, Republic of Korea; kscha@kitech.re.kr
[2] School of Mechanical Engineering, Yeungnam University, Gyeongsan 38541, Republic of Korea; jaehyun@yu.ac.kr
[3] Department of Automotive Engineering, Hanyang University, Seoul 04763, Republic of Korea; supertramph@hanyang.ac.kr
[4] Department of Mechanical, Robotics, and Energy Engineering, Dongguk University, Seoul 04620, Republic of Korea
* Correspondence: myungseop@hanyang.ac.kr (M.-S.L.); parksh@dgu.ac.kr (S.-H.P.)
† These authors contributed equally to this work.

Abstract: The fuel economy of electric vehicles (EVs) is an important factor in determining the competitiveness of EVs. Since the fuel economy is affected by the efficiency of an e-powertrain composed of a motor and inverter, it is necessary to select a high-efficiency topology for the e-powertrain. In this paper, a novel topology of e-powertrains to improve the fuel economy of EVs is proposed. The proposed topology aims to improve the system efficiency by integrating open-end winding (OEW) and winding changeover (WC). The proposed OEW-PMSM with WC enables to drive a permanent magnet synchronous motor (PMSM) in four different modes. Each mode can increase inverter efficiency and motor efficiency by changing motor parameters and maximum modulation index. In this paper, the system efficiency of the proposed topology was evaluated using electromagnetic finite element analysis and a loss model of power semiconductors. In addition, the vehicle simulations were performed to evaluate the fuel economy of the proposed topology, thereby proving the superiority of the proposed topology compared with the conventional PMSM.

Keywords: electric vehicles; fuel economy; open-end winding; permanent magnet synchronous motors; winding changeover

MSC: 65M80

Citation: Cha, K.-S.; Kim, J.-H.; Hwang, S.-W.; Lim, M.-S.; Park, S.-H. High-Efficiency e-Powertrain Topology by Integrating Open-End Winding and Winding Changeover for Improving Fuel Economy of Electric Vehicles. *Mathematics* **2024**, *12*, 3415. https://doi.org/10.3390/math12213415

Academic Editor: Bruno Antonio Pansera

Received: 4 October 2024
Revised: 25 October 2024
Accepted: 29 October 2024
Published: 31 October 2024

1. Introduction

As the era of electric vehicles (EVs) progresses beyond hybrid electric vehicles (HEVs), the demand for high-performance powertrains is increasing [1,2]. In the 2020s, the EV market is expanding not only in Europe but also in the Americas and Asia. Consequently, the demand for traction motors, a key component of EVs, is rising rapidly. Various types of traction motors exist, including induction motors, switched reluctance motors, and wound-field synchronous motors. Among these, permanent magnet synchronous motors (PMSMs) are the most commonly used for traction applications.

PMSMs offer the advantage of operating across a wide speed range with high efficiency, thanks to the use of high-energy-density rare earth permanent magnets (PMs). Since the performance of PMs is affected by temperature variations, the efficiency and heat dissipation characteristics are crucial for traction motors [3]. Additionally, energy losses occur in power semiconductors, such as insulated gate bipolar transistors (IGBTs), during the power conversion process, as the traction motor consumes energy stored in the

battery [4]. Therefore, both the efficiency of the inverter and the traction motor influence the overall mileage of EVs.

In order to improve the efficiency of the system consisting of traction motor and inverter, research has been conducted in various aspects in point view of traction motors and inverters. To increase the efficiency of traction motors, various winding technologies and design techniques have been proposed. Hairpin winding, which is widely used in traction motors with distributed winding, is a technology that maximizes current capacity and heat dissipation characteristics by improving the slot fill factor [5–7]. But the hairpin winding can only be adopted in distributed winding, so additive manufacturing-based winding technology for high fill factor concentrated winding is widely studied [8–11]. Additive manufacturing is effective in maximizing the fill factor of the coil but has a limitation in reducing DC resistance because the copper alloy used for laser forming has a higher resistivity than pure copper.

Although the increased conductor area has enhanced the efficiency of traction motors, further improvements in EV mileage can be achieved by optimizing the traction motor considering the vehicle's driving cycle [12–15]. Hwang et al. proposed an analysis method to predict fuel economy based on the driving cycle by coupling electromagnetic and thermal analysis, accounting for temperature variations in traction motors [12]. Sun et al. introduced a design optimization process for four-wheel-drive in-wheel motors, considering the driving cycle. As in-wheel motors operate close to direct-drive, they proposed a design approach for outer rotor PMSMs, focusing on low-speed, high-torque characteristics [13].

Flux-weakening (FW) control is essential for driving traction motors at high speeds within the constraints of limited battery voltage. When d-axis current is injected for FW control, the increased armature current leads to additional electromagnetic losses. In order to overcome the limited battery voltage, various overmodulation strategies have been studied to maximize the power density of the motor [16–18]. Overmodulation allows the traction motor to operate at higher voltages but does not provide a dramatic voltage increase because the voltage increase effect is less than 5%.

Therefore, it is effective to increase the battery voltage by adding battery cells to effective improve the efficiency of the drive motor. However, this approach is not recommended, as it increases the weight and cost of EVs. To address this, a topology of open-end winding PMSMs (OEW-PMSMs) has been proposed to boost the line-to-line voltage while maintaining the limited battery voltage [19–21]. OEW-PMSMs can operate with reduced d-axis current at high speeds due to the higher voltage limits. However, OEW-PMSMs require an additional power module, as the three-phase winding ends are fed by dual inverters that share the same battery source. A method utilizing wide-bandgap switches to mitigate the additional inverter losses from added power modules has been proposed [22,23]. However, this approach increases costs due to the use of wide-bandgap switches, limiting its adoption in the industry.

In cases where wide-bandgap switches cannot be used, effective control of the power module becomes crucial to reducing inverter losses. Several control techniques for OEW-PMSMs have been proposed to help reduce inverter losses. A key challenge in applying OEW-PMSMs is managing the zero-sequence current, which arises from the potential difference between inverters and the 3n-th flux linkage of the traction motor [24]. Various PWM techniques have been investigated to minimize common-mode voltage and suppress zero-sequence current. Park et al. proposed an effective solution for minimizing the common-mode voltage [25–27].

Winding changeover (WC) is a method that can drive the traction motor in two modes by changing the wiring of the armature winding [28,29]. By using the WC, high efficiency drive in a wide speed range can be achieved only by wiring the armature winding without any physical change of the traction motor. However, the large surge voltage generated during winding switching can damage the winding, necessitating the development of an appropriate switching technique to mitigate this surge voltage [30,31].

Therefore, this paper proposes a novel powertrain topology integrating OEW-PMSMs and WC for high-efficiency operation in the entire speed range. The proposed topology drives the traction motor in four modes, combining three-phase OEW conversion of the inverter and series-parallel conversion of the armature winding [32]. As a result of using the proposed topology, the fuel economy of EVs can be improved compared with the conventional three-phase topology.

Winding changeover (WC) is a method that enables traction motors to operate in two modes by reconfiguring the armature winding connections [28,29]. By utilizing WC, high-efficiency operation across a wide speed range can be achieved through simple wiring changes to the armature winding without any physical modifications to the traction motor. This paper proposes a novel powertrain topology that integrates OEW-PMSM and WC to achieve high efficiency across the entire speed range. The proposed topology allows the traction motor to operate in four modes by combining three-phase to OEW conversion with series-parallel conversion of the armature winding [32]. By employing this topology, the fuel economy of EVs can be improved compared with conventional three-phase systems.

2. Mathematical Model of OEW-PMSM

2.1. Characteristics of OEW-PMSMs

Figure 1a,b show the schematic of the OEW-PMSMs and their corresponding space vector voltage. In this topology, the armature windings of the PMSMs are not interconnected, which is why it is referred to as an open-end winding. Each end of the winding is powered by a separate inverter. The voltages of the PMSMs are determined by the space vector voltage of each inverter, as shown in Figure 1b. The three-phase voltages can be expressed as the difference between the voltages supplied by each inverter, as follows:

$$\begin{cases} v_u = v_{u1} - v_{u2} \\ v_v = v_{v1} - v_{v2} \\ v_w = v_{w1} - v_{w2} \end{cases} \quad (1)$$

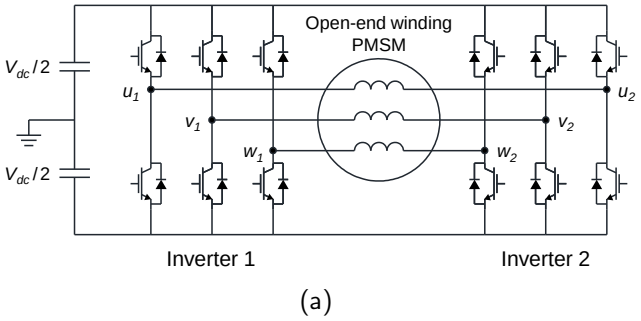

(a)

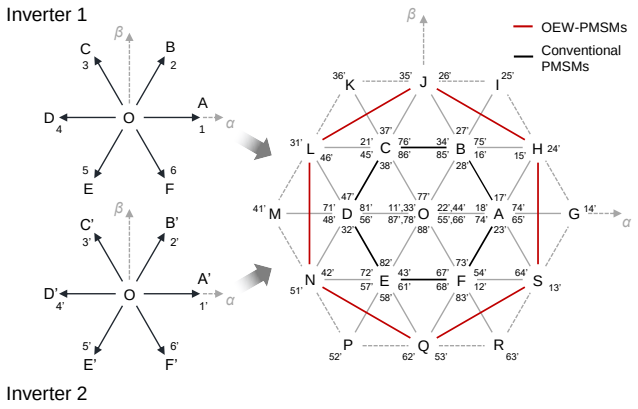

(b)

Figure 1. Schematic of (**a**) dual inverter fed OEW-PMSM and (**b**) hexagonal modulation diagram.

The voltage vectors from each inverter have a phase difference of 120° to supply the maximum voltage to the armature winding of PMSM. As a result, the maximum modulation index of the OEW-PMSMs can be increased compared with conventional three-phase PMSMs, as shown in Figure 1b. This feature allows the OEW-PMSMs to supply a higher line-to-line voltage to the conventional PMSMs, even with the limited battery voltage available in EVs.

To achieve high power density in a PMSM within a limited voltage, FW control, accomplished by injecting negative *d*-axis current, is required. Figure 2 illustrates the current vector for FW control in both conventional PMSMs and OEW-PMSMs. In conventional PMSMs, driving with FW control increases electromagnetic losses due to the higher armature current. However, by adopting the OEW topology, it is possible to achieve the same power density with a smaller *d*-axis current, thanks to the increased voltage capacity. As a result, the power density of the PMSMs can be enhanced, and the efficiency improved, compared with conventional PMSMs, due to the increased modulation index offered by the OEW topology.

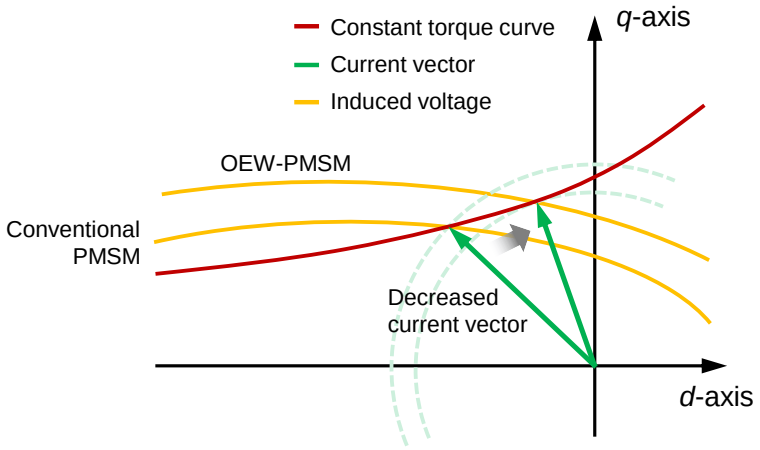

Figure 2. Comparison of current vector for flux-weakening control between conventional three-phase PMSMs and OEW-PMSMs.

When OEW is applied to PMSMs, the power density increases in proportion to the increased modulation index. However, since the load required for EV traction remains constant, the increased power density of OEW-PMSM is not necessary. Therefore, the number of series turns per phase for the OEW-PMSM should be increased by the same ratio as the increased modulation index to maintain the desired power density, as shown in Figure 3. By increasing the series turns per phase while maintaining the current density and slot fill factor, the peak current of the OEW-PMSM is reduced compared with that of a conventional PMSM as

$$i_{pk} = \frac{A_{slot} \cdot n_f \cdot J_{c,max}}{N_c} \tag{2}$$

As a result, the specifications of the OEW-PMSM and conventional PMSM are summarized in Table 1. Both the conventional PMSM and the OEW-PMSM are designed to drive 14.5 kW for personal mobility applications. Detailed specifications for personal mobility will be discussed in Section 5.

Table 1. The specifications of conventional PMSM and OEW-PMSM.

Item	Unit	Conventional	OEW-PMSM
Motor type	-	IPMSM	IPMSM
Number of poles/slots	-	16/24	16/24
Max. power	kW	14.5	14.5
Peak torque	Nm	50.0	50.0
DC link voltage	V_{DC}	72	72
Max. line-to-line voltage	-	$V_{DC}/\sqrt{3}$	V_{DC}
Series turns per phase	-	26	45
Number of parallel circuits	-	8	8
Temperature	°C	60	60

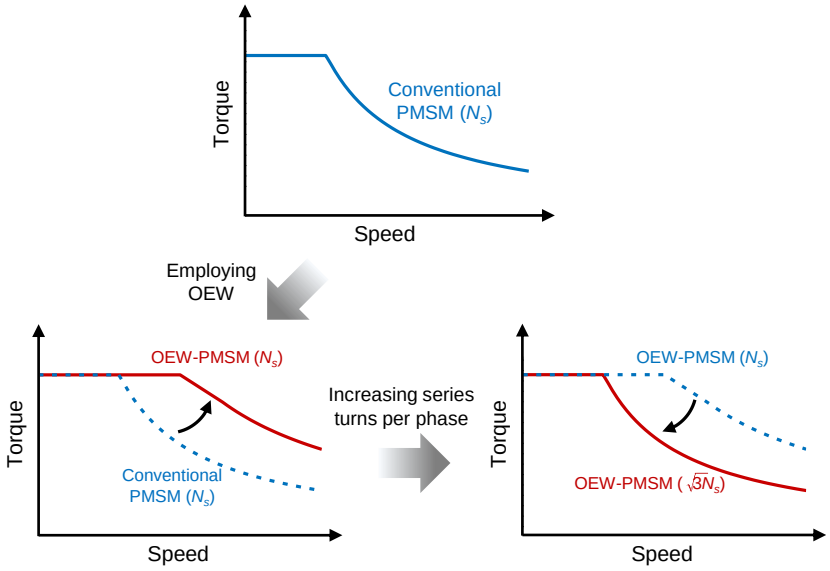

Figure 3. Comparison of torque-speed curve between OEW-PMSM and conventional PMSM for maintaining power density.

2.2. System Efficiency of OEW-PMSM

Since the motor system comprises both an inverter and a motor, the overall system efficiency is influenced by the efficiencies of both components. Unlike conventional PMSMs, OEW-PMSMs are driven by dual inverters, so the system efficiency of the OEW-PMSM must be calculated with consideration for the dual inverter drive.

The efficiency of the PMSM is determined by several factors, including the copper loss of the armature winding, the iron loss of the core material, the eddy current loss of the permanent magnets (PMs), mechanical losses from the bearings, and the mechanical power output. In this paper, the eddy current loss of the PMs is considered negligible. Additionally, the zero-sequence current, which poses a practical challenge in OEW applications, is not addressed in this study. Consequently, the total power loss of the motor, P_{mt}, can be calculated as follows:

$$P_{mt} = P_c + P_i + P_{mech} \tag{3}$$

The copper loss is determined by the electrical resistance of the armature winding and armature current, and the armature current can be modeled as

$$R_a = \rho_c \frac{N_s}{N_p} \frac{(L_{stk} + l_{end})N_c^2}{A_{slot} \cdot n_f} \tag{4}$$

Then, the copper loss can be calculated using (2) and (4) as

$$P_c = 3\rho_c \frac{N_s(L_{stk} + l_{end})A_{slot} \cdot n_f \cdot J_c}{N_p} \tag{5}$$

Thus, the copper loss is influenced by the size of the motor and the magnetomotive force (MMF) of the armature winding. Since the MMF for both conventional PMSM and OEW-PMSM is the same at the same torque and speed, the copper losses for each motor are also identical. Additionally, the iron loss of the PMSM is determined by the MMF of the armature winding and the frequency of the magnetic flux density; therefore, the iron losses of both conventional PMSMs and OEW-PMSMs are the same under the same operating conditions. Consequently, the efficiencies of the conventional PMSM and OEW-PMSM are equivalent.

The efficiency of inverters is determined by the power loss of IGBTs and diodes. The power loss of IGBTs and diodes can be divided into conduction loss and switching loss. Each loss can be modeled as follows [33].

$$P_{c,T} = \left(\frac{1}{2\pi} + \frac{M\cos(\phi)}{8}\right)V_{ce0}I_1 + \left(\frac{1}{8} + \frac{M\cos(\phi)}{3\pi}\right)r_{ce}I_1^2 \tag{6}$$

$$P_{sw,T} = f_{sw}\frac{E_{on}(I_1) + E_{off}(I_1)}{\pi} \tag{7}$$

$$P_{c,D} = \left(\frac{1}{2\pi} + \frac{M\cos(\phi)}{8}\right)V_{F0}I_1 + \left(\frac{1}{8} - \frac{M\cos(\phi)}{3\pi}\right)r_F I_1^2 \tag{8}$$

$$P_{sw,D} = f_{sw}\frac{E_{rr}(I_1)}{\pi} \tag{9}$$

The characteristics of IGBT and diode for calculating the power loss can be derived from the datasheet, as shown in Figure 4a–d [34].

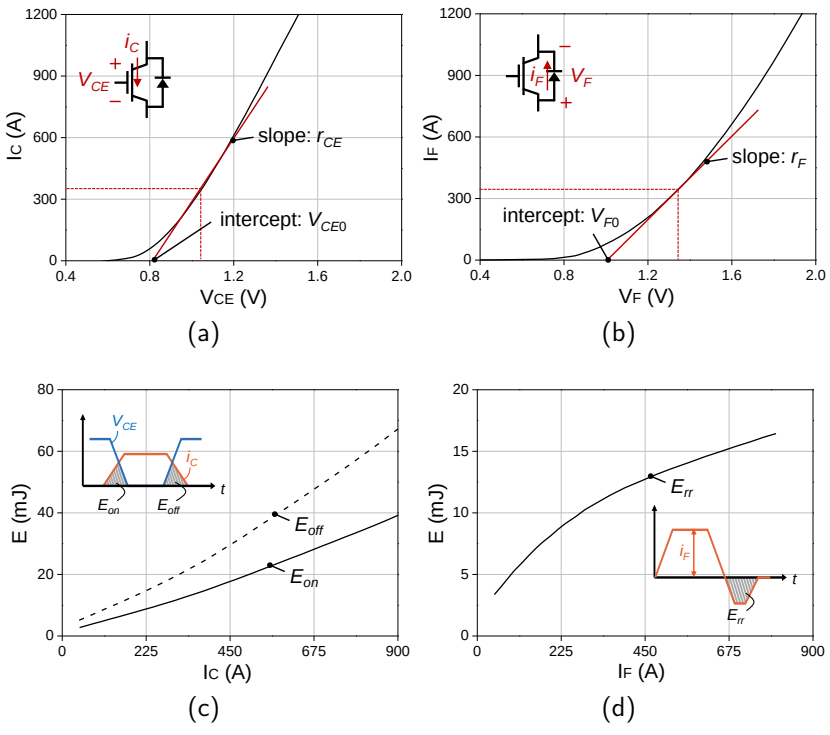

Figure 4. Characteristics and switching loss of power semiconductors: (**a**) Characteristics of IGBT, (**b**) diode and switching loss of (**c**) IGBT, (**d**) diode.

The conduction loss of the inverter is influenced by power factor, induced voltage, and phase current. For the OEW-PMSM, the conduction loss of a single IGBT and diode is lower than that of the conventional PMSM. The switching loss for a single IGBT and diode in both topologies is equivalent, as the switching frequencies are the same for each. Therefore, the total power loss of the conventional three-phase inverter can be calculated as follows:

$$P_{inv} = 6(P_{c,T} + P_{sw,T} + P_{c,D} + P_{sw,T}) \tag{10}$$

However, the dual inverter topology of the OEW-PMSM utilizes twice as many IGBTs and diodes compared with the conventional three-phase inverter. This difference must be taken into account when calculating the efficiency of the inverter. Additionally, the conduction loss for each inverter should be calculated while considering their respective power factors, as illustrated in Figure 5. Finally, the system efficiency of the OEW-PMSM can be calculated as follows:

$$\eta_{sys,OEW} = \eta_{inv,OEW} \cdot \eta_{mt,OEW} \tag{11}$$

where

$$\eta_{inv,OEW} = \frac{P_{out} + P_{mt}}{P_{out} + P_{mt} + P_{inv1} + P_{inv2}} \tag{12}$$

$$\eta_{mt,OEW} = \frac{P_{out}}{P_{out} + P_{mt}} \tag{13}$$

By using the system efficiency of OEW-PMSM, the system efficiency of proposed topology can be calculated.

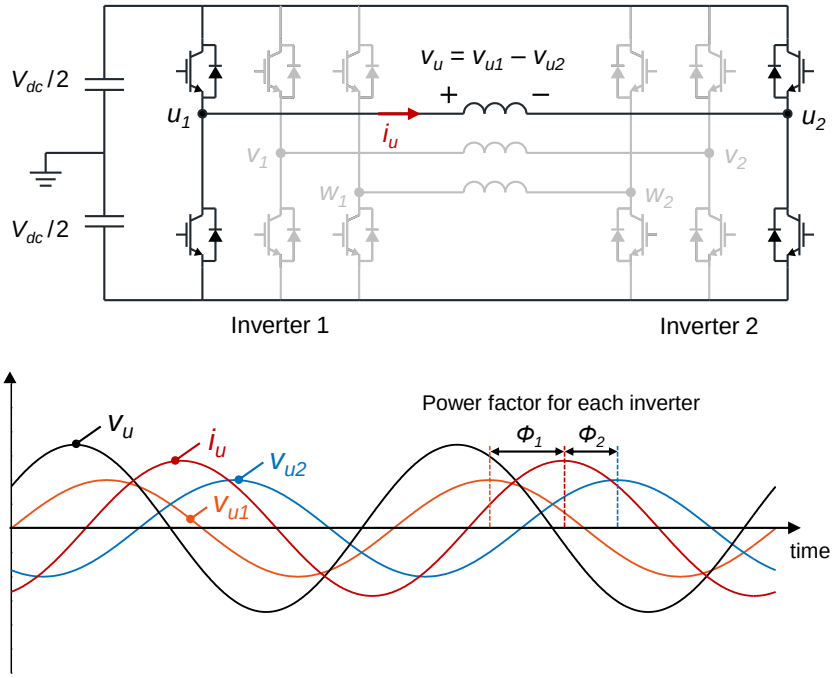

Figure 5. Power factor between armature current and reference voltage from each inverter.

3. Characteristics of OEW-PMSM with Winding Changeover

3.1. Operation in Series-Parallel Mode

The electromagnetic performance of PMSMs is highly dependent on the number of series turns per phase. If the slot fill factor and current density remain constant, the peak current and power density of the PMSMs decrease as the number of series turns per phase increases, while they increase when the number of series turns per phase decreases. Winding changeover (WC) allows for the adjustment of the series turns per phase by converting the armature winding between series and parallel configurations [28,29]. Figure 6a presents

an example circuit for implementing the WC. The coil is divided into two parts for converting the armature winding, and switches for series and parallel modes are installed for each phase. In series mode, the middle switch is closed while the switches on both sides are open, connecting the two windings in series. In parallel mode, the switches operate in the opposite manner, connecting the two windings in parallel. Consequently, the armature current flows differently in each mode, as illustrated in Figure 6b.

When the armature winding of the PMSM operates in series and parallel modes, the number of series turns per phase is doubled in series mode compared with parallel mode. Since the resistance and d, q-axis inductance are proportional to the square of the number of series turns per phase, while the flux linkage is directly proportional to the number of series turns per phase, the motor parameters can be expressed as follows, depending on the operation mode.

$$R_{a,s} = (1 + S_{wc})^2 R_{a,p} \tag{14}$$

$$L_{dq,s} = (1 + S_{wc})^2 L_{dq,p} \tag{15}$$

$$\psi_{a,s} = (1 + S_{wc}) \psi_{a,p} \tag{16}$$

Therefore, the motor parameters change according to the WC operation mode.

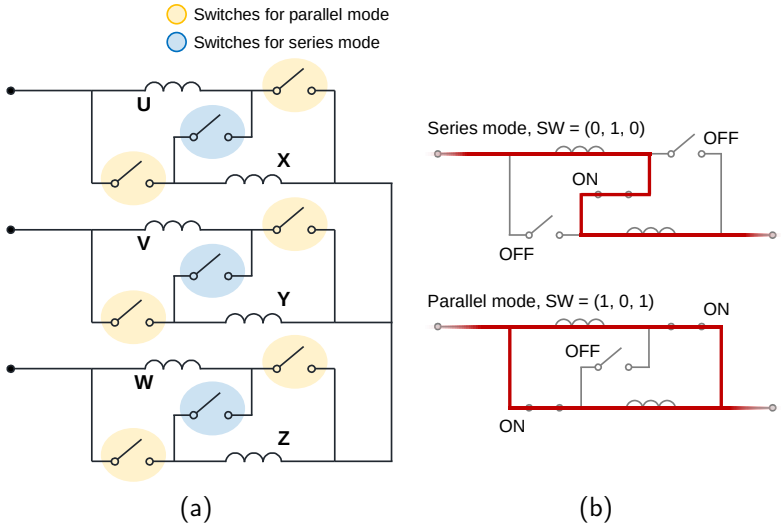

Figure 6. Principle of the winding changeover. (**a**) Example circuit for winding changeover and (**b**) current flow in series and parallel mode.

Figure 7a,b illustrates the electromagnetic performance of the conventional PMSM when it is operated in each mode. Assuming that the peak current of the inverter remains constant, the torque density in series mode is improved in the low-speed region compared with parallel mode due to the increased flux-linkage. Conversely, high power density can be achieved in parallel mode, thanks to the reduced impedance of the motor. Additionally, since the d-axis current for FW control is lower in parallel mode than in series mode, efficiency can be enhanced by minimizing copper and iron losses.

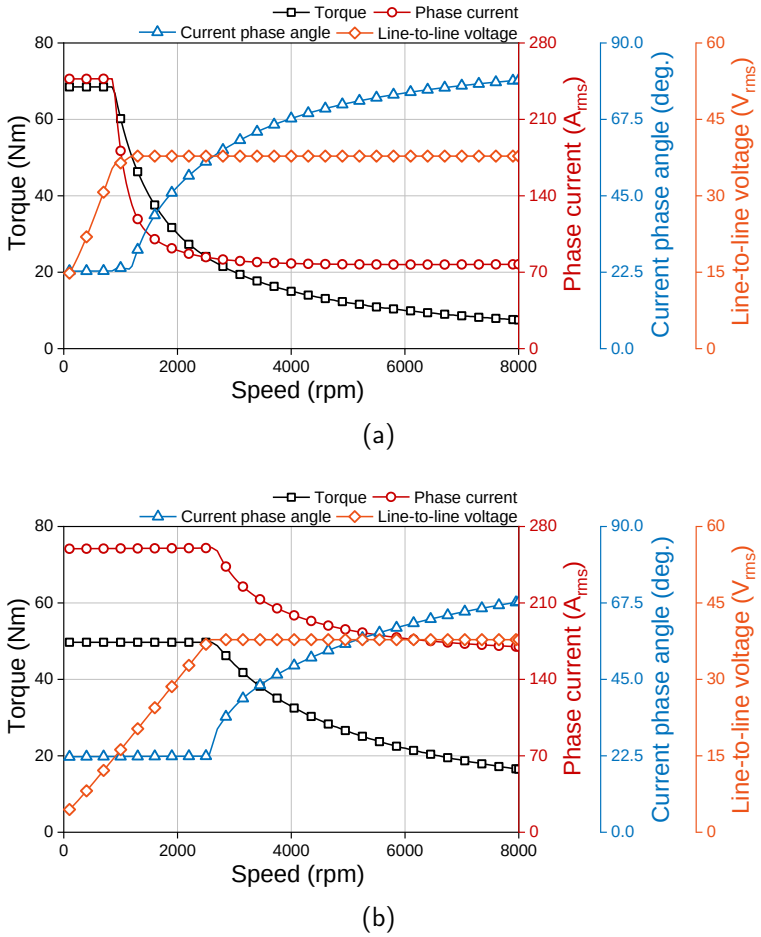

Figure 7. Electromagnetic characteristics of conventional PMSM with (**a**) series mode and (**b**) parallel mode.

3.2. Proposed OEW-PMSM with WC

By leveraging the advantages of OEW and WC, we propose a novel topology that facilitates high-efficiency operation across the entire speed range for EV traction. Figure 8 presents the schematic of the proposed topology. To implement WC, the windings of the PMSM are separated, and the ends of each phase are left unconnected for dual inverter drive. This proposed topology enables the PMSM to operate in four modes by integrating series and parallel configurations with three-phase and dual inverter drives, as illustrated in Figure 9.

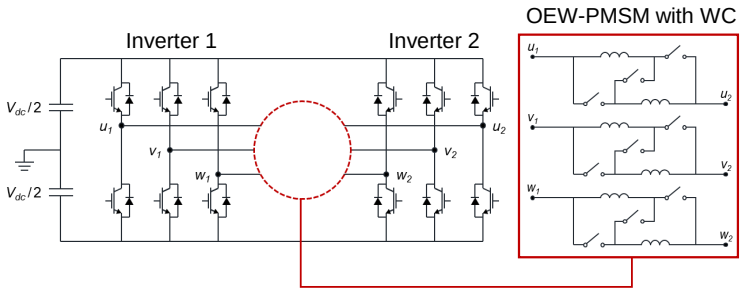

Figure 8. Schematic of proposed OEW-PMSM with WC.

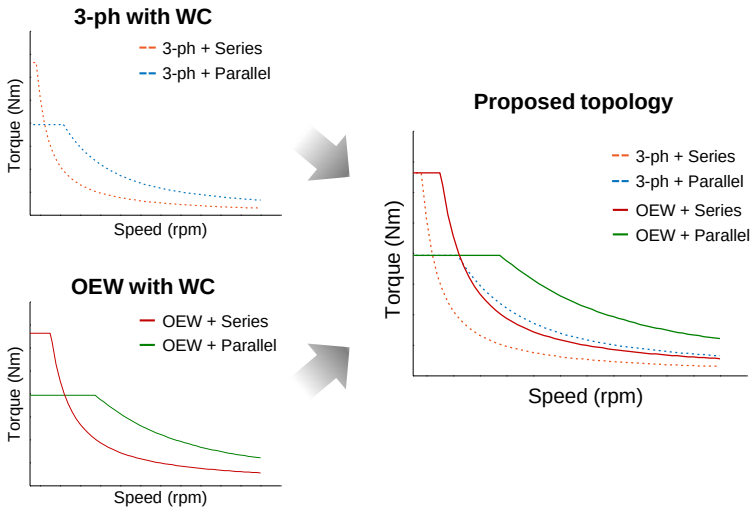

Figure 9. Operation range of proposed topology.

Since the maximum modulation index and motor parameters vary with the operating mode, the system efficiency for each speed region also changes accordingly. When the proposed topology operates in three-phase mode with WC, the system efficiency in the low-speed region can be enhanced because the motor runs on a single inverter with a low armature current. However, in the high-speed region, system efficiency may decrease due to the FW control, which is limited by the lower modulation index. Conversely, when the proposed topology operates in OEW mode with WC, the system efficiency in the high-speed region can be improved, as a lower *d*-axis current is needed to drive the motor effectively due to the higher modulation index.

4. Mode Selection Strategy for High System Efficiency

As the proposed topology provides four modes, which are series mode with three-phase, parallel mode with three-phase, series mode with OEW, and parallel mode with OEW, an effective strategy for selecting the operating mode should be required. In this paper, the strategy illustrated in Figure 10 is adopted to maximize the system efficiency of the proposed topology. When the torque and speed are specified, the system efficiency for each operating mode is derived by calculating the motor parameters based on the series-parallel configuration. The system efficiency is determined by considering the maximum modulation index for either the three-phase or OEW drive. Consequently, the OEW-PMSM operates in the mode that yields the highest system efficiency.

Figure 11a–d presents the efficiency map of the motor for each mode. In this analysis, the specifications of PMSM from Table 1 were used to verify the performance of the proposed topology. When the PMSM operates in OEW mode, power density increases compared with three-phase mode due to the higher modulation index. In contrast, while operating in series mode, power density decreases because of increased impedance, although the peak torque increases. In the low-speed region, there is no significant difference in motor efficiency between three-phase and OEW modes, as the required modulation index is small. However, in the high-speed region, the motor efficiency in three-phase mode decreases due to FW control. Additionally, when the PMSM operates in series mode, high-speed efficiency is also reduced because of the increased impedance associated with FW control.

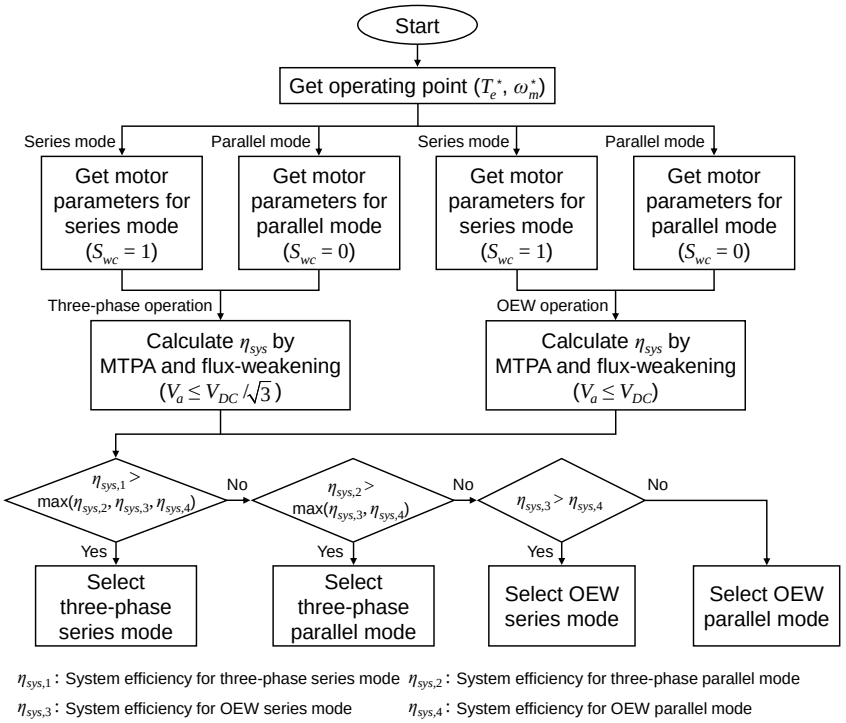

Figure 10. Algorithm for selecting operation mode to achieve high system efficiency drive.

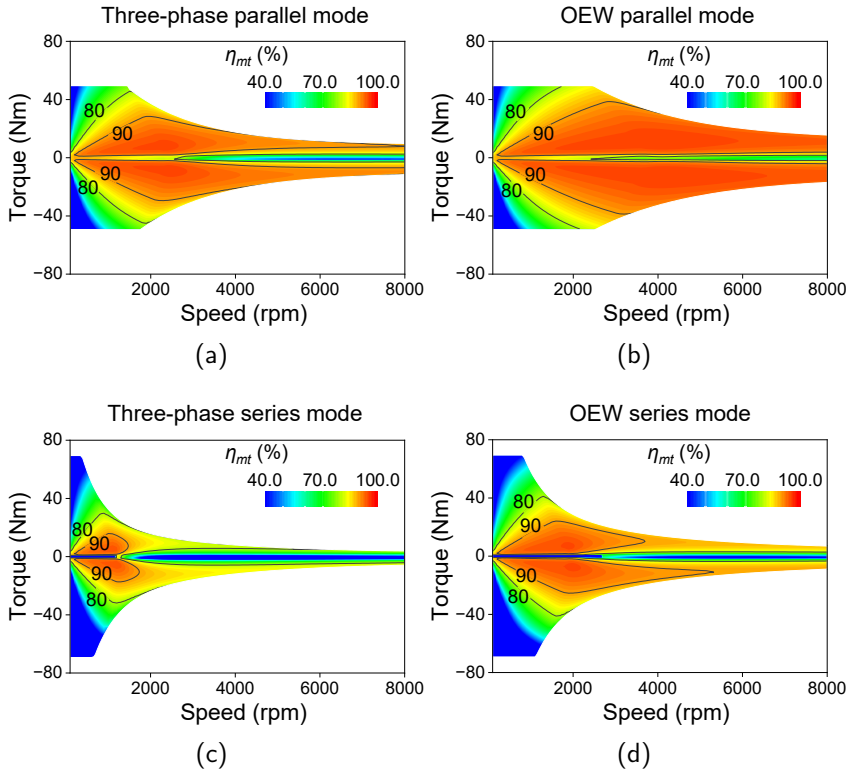

Figure 11. Motor efficiency map for (**a**) three-phase parallel mode, (**b**) OEW parallel mode, (**c**) three-phase series mode, and (**d**) OEW series mode.

Figure 12a–d presents the inverter efficiency maps for each mode. When the PMSM operates in OEW mode, the inverter efficiency is lower than that of three-phase mode due to the increased number of IGBTs and diodes. Furthermore, the inverter efficiency in series

mode is higher than in parallel mode because the conduction losses of the IGBT and diode decrease as the armature current reduces in the low-speed region.

The system efficiency map of the PMSM based on the operating mode is shown in Figure 13a–d. By considering both the efficiency of the motor and the inverter, the system efficiency varies according to the speed and torque ranges. Utilizing the algorithm illustrated in Figure 10, the proposed topology can operate with high system efficiency, as depicted in Figure 14.

In Section 1, which represents the low-speed, high-torque region, the system operates in three-phase series mode to maximize efficiency by reducing the armature current with a single inverter. Section 2 operates in OEW series mode to maintain base speed with high torque. Finally, Section 3 operates in OEW parallel mode to enhance system efficiency during high-speed operation.

Figure 15 illustrates the system efficiency map of the proposed topology. By operating in series mode in the low-speed region and in parallel mode in the high-speed region, the PMSM can achieve high system efficiency across the entire speed range. Generally, the main operating points of EVs are located in the low-speed, high-torque, and high-speed, low-torque regions, making the proposed topology advantageous for improving vehicle mileage. Figure 16 highlights the difference in system efficiency between the conventional PMSM and the proposed topology. In the low-speed region, the use of series mode with a single inverter significantly enhances system efficiency. However, in the high-speed region, the system efficiency of the proposed topology is lower than that of the conventional PMSM due to its reliance on dual inverters.

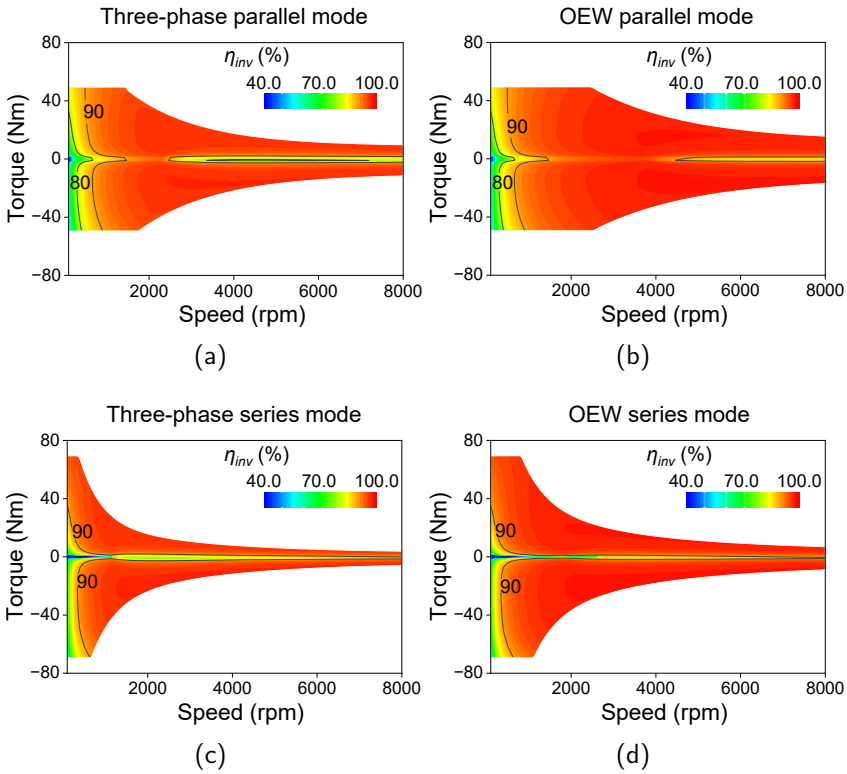

Figure 12. Inverter efficiency map for (**a**) three-phase parallel mode, (**b**) OEW parallel mode, (**c**) three-phase series mode, and (**d**) OEW series mode.

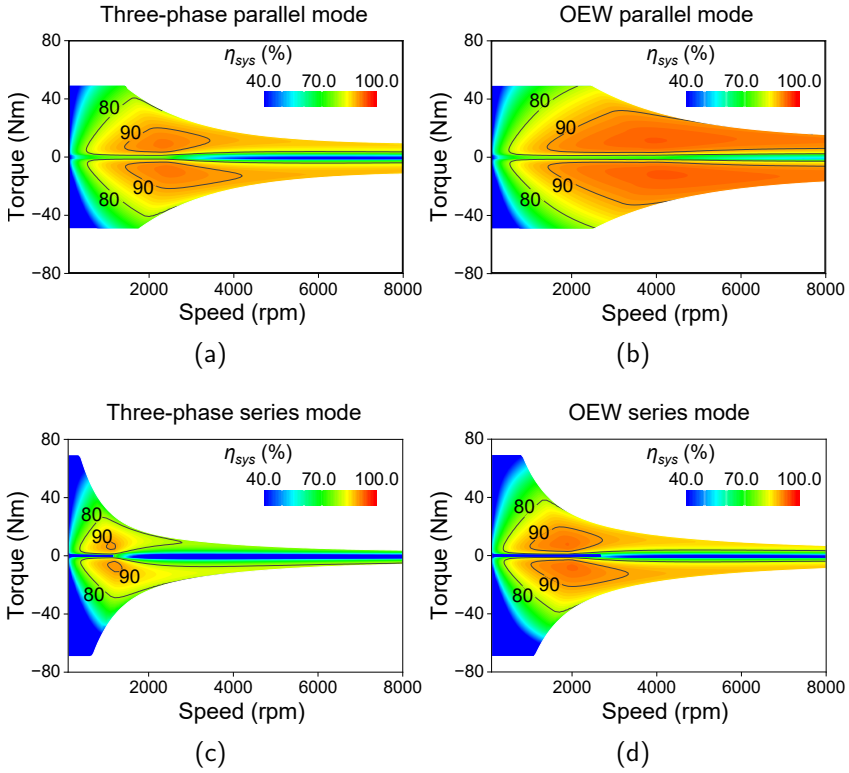

Figure 13. System efficiency map for (**a**) three-phase parallel mode, (**b**) OEW parallel mode, (**c**) three-phase series mode, and (**d**) OEW series mode.

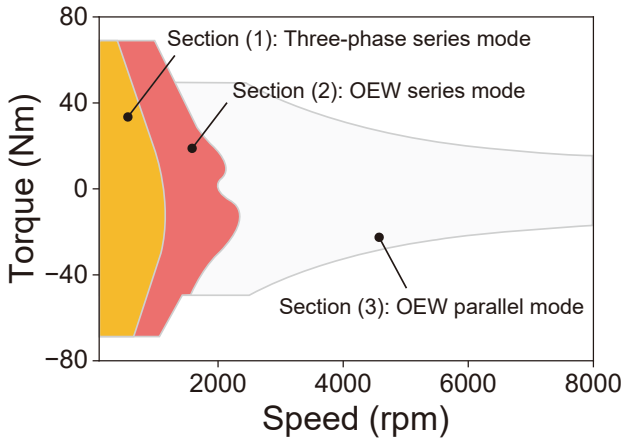

Figure 14. Operation mode of proposed topology to maximize the system efficiency.

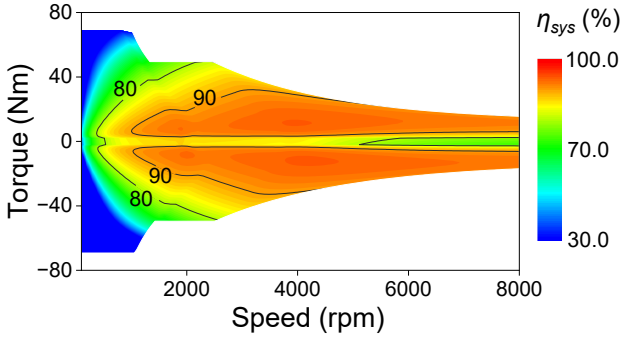

Figure 15. Integrated system efficiency map of proposed topology.

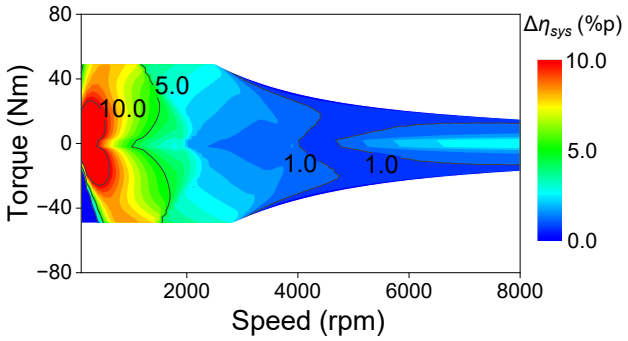

Figure 16. Difference of system efficiency map between conventional PMSM and proposed topology.

5. Fuel Economy of Electric Vehicle Using OEW-PMSM with WC

To calculate the fuel economy of the EV, vehicle simulations were conducted in this section using the advanced vehicle simulator (ADVISOR) developed by the National Renewable Energy Laboratory [35]. The target vehicle is a 10.2 kW personal mobility unit, and the driving cycle was set to the New York City Cycle (NYCC), as shown in Figure 17a, which is well-suited for personal mobility applications. Since the NYCC mimics urban driving conditions, it emphasizes low-speed driving rather than high-speed performance. The schematic of the vehicle simulations is illustrated in Figure 18. These simulations aim to assess the fuel economy of the vehicle based on two e-powertrain systems: the conventional three-phase PMSM and the proposed topology. The total resistance force acting on the vehicle comprises rolling resistance, grading resistance, and aerodynamic drag, as follows:

$$\begin{aligned} F_{r,total} &= F_R + F_G + F_D \\ &= f_R M_v g \cos\theta + M_v g \sin\theta + \frac{1}{2}\rho_{air} A_f C_D (V_v + V_w)^2 \end{aligned} \tag{17}$$

Then, the motion of the vehicle is determined by the traction force of the e-powertrain and resistance force as

$$M_v a_v = F_t - F_{r,total} \tag{18}$$

Finally, the traction torque of the e-powertrain can be calculated when the vehicle is driven along the driving cycle as

$$T_m^* = \frac{r_w F_t}{n_G \eta_G} \tag{19}$$

Since the NYCC includes numerous stop-and-go situations, as shown in Figure 17b, the e-powertrain is frequently operated in low-speed and high-torque. The detailed specifications of the vehicle and driving conditions are listed in Table 2. In this paper, temperature variations of the PMSM and inverter during the driving cycle are not considered. A comparison of fuel economy was conducted under the assumption that the average temperature during driving conditions aligns with the temperature values presented in Table 1.

Table 2. The specifications of vehicle and driving conditions.

Item	Unit	Value
Curb weight	kg	474
Frontal area	m^2	1.8
Wheel size	in	13
Tire size	-	125/80R13
Gear ratio	-	15.0
Gear efficiency	%	95
Battery capacity	kWh	6.1
ρ_{air}	kg/m^2	1.2
C_D	-	0.64
f_r	-	0.01

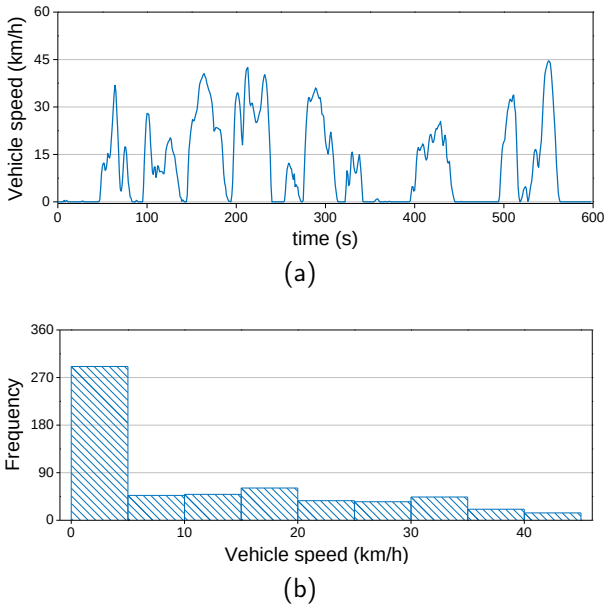

Figure 17. Target driving cycle that is suitable for personal mobility: (**a**) waveform of vehicle speed and (**b**) vehicle speed distribution of NYCC cycle.

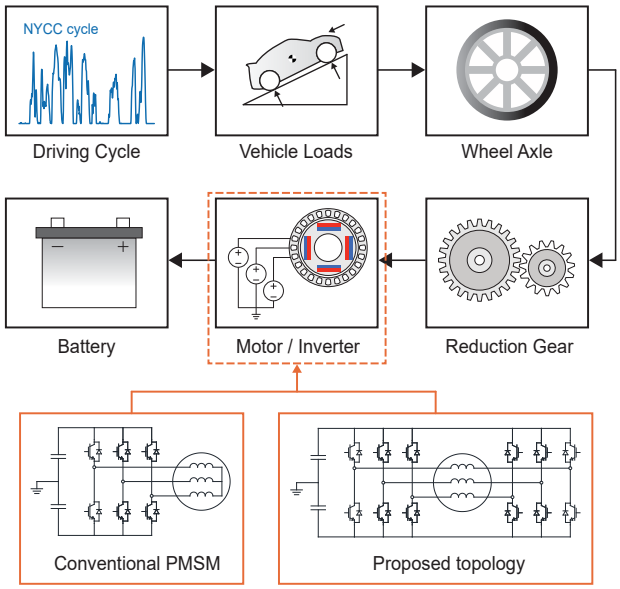

Figure 18. Target driving cycle that is suitable for personal mobility.

Figure 19a,b show the operating points of the traction motor over the torque-speed curve for each topology. The operating points required to overcome the total resistance force while driving under the NYCC are located on the torque-speed curve of the traction motor. These operating points are positioned near the low-speed, high-torque region, which is characteristic of urban driving cycles that involve frequent acceleration and deceleration. Therefore, the proposed topology, which significantly enhances system efficiency in the low-speed, high-torque region, offers advantages in fuel economy compared with the conventional PMSM.

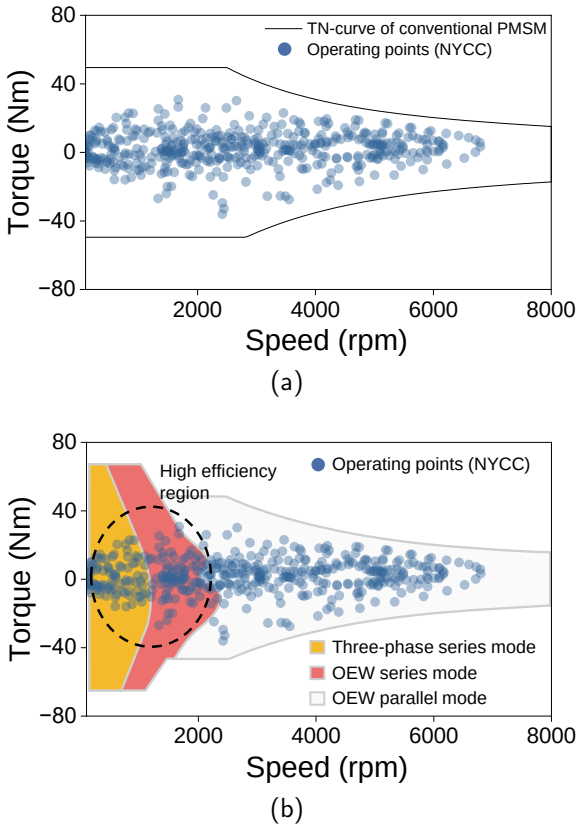

Figure 19. Operation points of traction motor and TN-curve for (**a**) conventional PMSM and (**b**) proposed topology.

Figure 20a–d presents a comparison of the simulation results for power consumption during the driving cycle for each e-powertrain topology. The rotational speed and controlled torque of the motor are shown in Figure 20a,b. As the motor is frequently operated in low-speed regions, the system loss of the proposed topology is much lower than that of the conventional PMSM throughout the entire driving cycle, as shown in Figure 20c. Because of the difference in system loss between each topology, the consumed energy of the proposed topology is much higher than that of the conventional topology throughout the driving cycle, as shown in Figure 20d. Consequently, the total consumed energy of the proposed topology is 3.9% lower than that of the conventional PMSM, as shown in Figure 21a, and the fuel economy of the proposed topology is 4.1% higher than that of the conventional PMSM, as shown in Figure 21b.

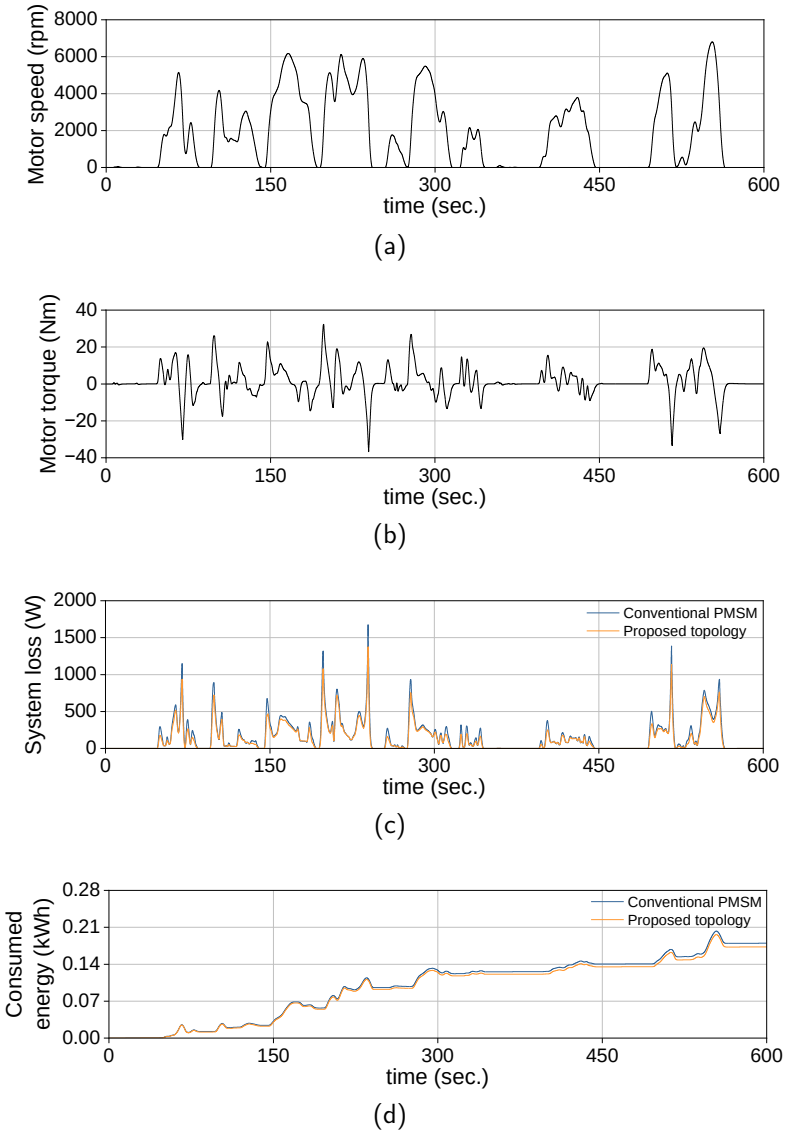

Figure 20. Comparison of energy consumption for driving cycle according to the e-powertrain topology: (**a**) rotational speed of the motor, (**b**) controlled torque of motor, (**c**) comparison of system loss for each topology, and (**d**) comparison of consumed energy for each topology.

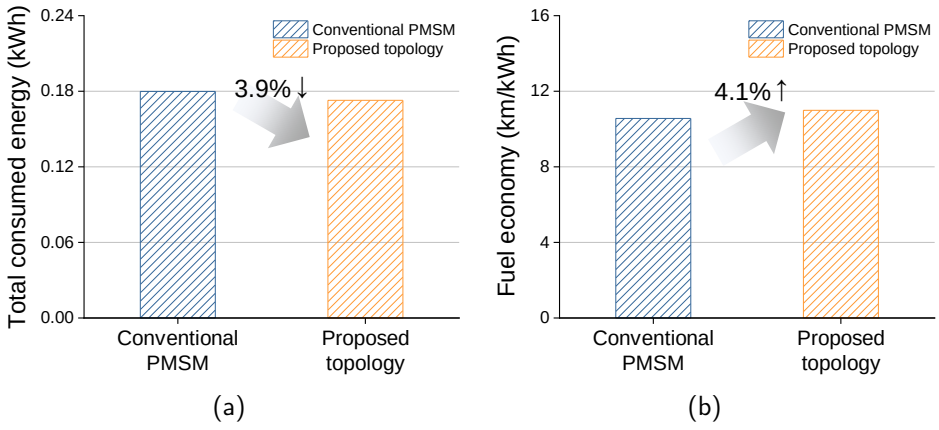

Figure 21. Comparison of total consumed energy and fuel economy according to the e-powertrain topology: (**a**) Comparison of total consumed energy and (**b**) fuel economy.

6. Conclusions and Future Works

This paper proposes a novel topology for e-powertrains to improve the fuel economy of electric vehicles. The proposed topology enables to drive the PMSM in four different modes by integrating OEW-PMSM and WC. By using the WC to change the impedance of PMSM and applying OEW to increase the maximum modulation index, a wide speed and torque range can be achieved. In order to analyze the system efficiency of the proposed topology, inverter losses due to phase current change during series and parallel mode conversion were evaluated, and a system efficiency evaluation method was proposed considering the dual inverter-fed OEW operation. In addition, an algorithm for selecting the operation mode for a high system efficiency drive was proposed, and the comparison of system efficiency between conventional 3-phase PMSM and the proposed topology was conducted. In addition, the vehicle simulations were performed for fuel economy analysis. As a result, the validity of the proposed topology was verified through simulations to improve fuel economy.

This research is about the feasibility validation of the proposed topology for improving the fuel economy of EVs. Therefore, the energy loss occurring in the switching circuit for OEW and WC and the cost increase effect for implementing the topology are not addressed in this paper. In addition, the effect of the zero-sequence current flowing through the dual inverter when applying OEW is not considered. Thus, we will conduct research to contribute to the commercialization of the proposed topology. In the future, we will build a prototype for experimental verifications, and switching circuits will be studied for implementing the OEW and WC topologies. Additionally, control techniques to suppress surge voltage for implementing OEW and WC will be studied together.

Author Contributions: Conceptualization, J.-H.K. and S.-H.P.; methodology, K.-S.C.; software, S.-H.P.; validation, S.-W.H.; resources, M.-S.L.; data curation, K.-S.C.; writing—original draft preparation, J.-H.K. and K.-S.C.; writing—review and editing, M.-S.L. and S.-H.P.; visualization, S.-H.P.; supervision, M.-S.L.; project administration, S.-W.H.; funding acquisition, M.-S.L. and S.-H.P. All authors have read and agreed to the published version of the manuscript.

Funding: This work was supported by the Dongguk University Research Fund of 2023 (S-2023-G0001-00095).

Data Availability Statement: Data are contained within the article.

Conflicts of Interest: The authors declare no conflicts of interest.

References

1. De Santiago, J.; Bernhoff, H.; Ekergård, B.; Eriksson, S.; Ferhatovic, S.; Waters, R.; Leijon, M. Electrical motor drivelines in commercial all-electric vehicles: A review. *IEEE Trans. Veh. Technol.* **2012**, *61*, 475–484. [CrossRef]
2. Sarlioglu, B.; Morris, C.T.; Han, D.; Li, S. Driving toward accessibility: A review of technological improvements for electric machines, power electronics, and batteries for electric and hybrid vehicles. *IEEE Trans. Ind. Appl.* **2017**, *23*, 14–25. [CrossRef]
3. Demetriades, G.D.; De La Parra, H.Z.; Andersson, E.; Olsson, H. A real-time thermal model of a permanent-magnet synchronous motor. *IEEE Trans. Power Electron.* **2010**, *25*, 463–474. [CrossRef]
4. Du, G.; Cao, W.; Hu, S.; Lin, Z.; Yuan, T. Design and assessment of an electric vehicle powertrain model based on real-world driving and charging cycles. *IEEE Trans. Veh. Technol.* **2019**, *68*, 1178–1187. [CrossRef]
5. Popescu, M.; Goss, J.; Staton, D.A.; Hawkins, D.; Chong, Y.C.; Boglietti, A. Electrical vehicles—Practical solutions for power traction motor systems. *IEEE Trans. Ind. Appl.* **2018**, *54*, 2751–2762. [CrossRef]
6. Berardi, G.; Bianchi, N. Design Guideline of an AC Hairpin Winding. In Proceedings of the 2018 XIII International Conference on Electrical Machines (ICEM), Alexandroupoli, Greece, 3–6 September 2018; pp. 2444–2450.
7. Park, H.J.; Lim, M.S. Design of high power density and high efficiency wound-field synchronous motor for electric vehicle traction. *IEEE Access* **2019**, *7*, 46677–46685. [CrossRef]
8. Wrobel, R.; Mecrow, B. A comprehensive review of additive manufacturing in construction of electrical machines. *IEEE Trans. Energy Convers.* **2020**, *35*, 1054–1064. [CrossRef]
9. Selema, A.; Ibrahim, M.N.; Sergeant, P. Metal additive manufacturing for electrical machines: Technology review and latest advancements. *Energies* **2022**, *15*, 1076. [CrossRef]
10. Selema, A.; Van Den Abbeele, J.; Ibrahim, M.N.; Sergeant, P. Innovative 3D Printed Coil and Cooling Designs for Weight-Sensitive Energy-Saving Electrical Machine. *IEEE Trans. Transp. Electrif.* **2023**, *10*, 5282–5293. [CrossRef]

11. Lizarribar, B.; Prieto, B.; Selema, A.; Ibrahim, M.N.; Sergeant, P.; Artetxe, G.; Martínez-Iturralde, M. Multiphysics topology optimization of aluminium and copper conductors for automotive electrical machines. *IEEE Trans. Transp. Electrif.* **2024**.. [CrossRef]
12. Hwang, S.W.; Ryu, J.Y.; Chin, J.W.; Park, S.H.; Kim, D.K.; Lim, M.S. Coupled electromagnetic-thermal analysis for predicting traction motor characteristics according to electric vehicle driving cycle. *IEEE Trans. Veh. Technol.* **2021**, *70*, 4262–4272. [CrossRef]
13. Sun, X.; Shi, Z.; Cai, Y.; Lei, G.; Guo, Y.; Zhu, J. Driving-cycle-oriented design optimization of a permanent magnet hub motor drive system for a four-wheel-drive electric vehicle. *IEEE Trans. Transp. Electrif.* **2020**, *6*, 1115–1125. [CrossRef]
14. Ahn, S.; Song, W.; Min, S. Multiobjective Optimization of a Traction Motor in Driving Cycles Using a Coupled Electromagnetic–Thermal 1D Simulation. *Int. J. Energy Res.* **2023**, *2023*, 8854778. [CrossRef]
15. Mahmouditabar, F.; Baker, N.J. Design Optimization of Induction Motors with Different Stator Slot Rotor Bar Combinations Considering Drive Cycle. *Energies* **2023**, *17*, 154. [CrossRef]
16. Zhang, Y.; Qi, R. High-efficiency flux weakening drive for IPMSM based on model predictive control. *IEEE Trans. Transp. Electrif.* **2022**, *8*, 3503–3511. [CrossRef]
17. Vera, L.J.F.C.; Hsieh, M.F. Investigating the Impact of Characteristic Current on IPMSM Efficiency Area in Flux-Weakening Region. *IEEE Trans. Magn.* **2024**, *60*, 8204006. [CrossRef]
18. Seok, J.K.; Kim, J.S.; Sul, S.K. Overmodulation strategy for high-performance torque control. *IEEE Trans. Power Electron.* **1998**, *13*, 786–792. [CrossRef]
19. Baiju, M.R.; Mohapatra, K.K.; Kanchan, R.S.; Gopakumar, K. A Dual Two-Level Inverter Scheme with Common Mode Voltage Elimination for an Induction Motor Drive. *IEEE Trans. Power Electron.* **2004**, *19*, 794–805. [CrossRef]
20. Hu, W.; Nian, H.; Sun, D. Zero-sequence current suppression strategy with reduced switching frequency for open-end winding PMSM drives with common DC bus. *IEEE Trans. Ind. Electron.* **2019**, *66*, 7613–7623. [CrossRef]
21. Lin, X.; Huang, W.; Wang, L. SVPWM strategy based on the hysteresis controller of zero-sequence current for three-phase open-end winding PMSM. *IEEE Trans. Power Electron.* **2019**, *34*, 3474–3486. [CrossRef]
22. Morya, A.K.; Gardner, M.C.; Anvari, B.; Liu, L.; Yepes, A.G.; Doval-Gandoy, J.; Toliyat, H.A. Wide bandgap devices in AC electric drives: Opportunities and challenges. *IEEE Trans. Transp. Electrif.* **2019**, *5*, 3–20. [CrossRef]
23. Chang, L.; Alvi, M.; Lee, W.; Kim, J.; Jahns, T.M. Efficiency optimization of PWM-induced power losses in traction drive systems with IPM machines using wide bandgap-based inverters. *IEEE Trans. Ind. Appl.* **2022**, *58*, 5635–5649. [CrossRef]
24. Zhan, H.; Zhu, Z.q.; Odavic, M. Analysis and suppression of zero sequence circulating current in open winding PMSM drives with common DC bus. *IEEE Trans. Ind. Appl.* **2017**, *53*, 3609–3620. [CrossRef]
25. Bodo, N.; Jones, M.; Levi, E. A space vector PWM with common-mode voltage elimination for open-end winding five-phase drives with a single DC supply. *IEEE Trans. Ind. Electron.* **2013**, *61*, 2197–2207. [CrossRef]
26. Belkhode, S.; Jain, S. Optimized switching PWM technique with common-mode current minimization for five-phase open-end winding induction motor drives. *IEEE Trans. Power Electron.* **2018**, *34*, 8971–8980. [CrossRef]
27. Hu, W.; Ruan, C.; Nian, H.; Sun, D. Zero-sequence current suppression strategy with common-mode voltage control for open-end winding PMSM drives with common DC bus. *IEEE Trans. Ind. Electron.* **2020**, *68*, 4691–4702. [CrossRef]
28. Lim, M.S.; Hong, J.P. Design of high efficiency wound field synchronous machine with winding connection change method. *IEEE Trans. Energy Convers.* **2018**, *33*, 1978–1987. [CrossRef]
29. Cha, K.S.; Kim, D.M.; Jung, Y.H.; Lim, M.S. Wound field synchronous motor with hybrid circuit for neighborhood electric vehicle traction improving fuel economy. *Appl. Energy* **2020**, *263*, 114618. [CrossRef]
30. Im, S.H.; Gu, B.G. A snubberless solid-state tap changer for permanent magnet synchronous motors. *IEEE Trans. Power Electron.* **2020**, *35*, 12143–12152. [CrossRef]
31. Swamy, M.M.; Kume, T.; Maemura, A.; Morimoto, S. Extended high-speed operation via electronic winding-change method for AC motors. *IEEE Trans. Ind. Appl.* **2006**, *42*, 742–752. [CrossRef]
32. Park, S.H.; Cha, K.S.; Hwang, S.W.; Kim, J.H.; Lim, M.S. Open-End Winding Permanent Magnet Synchronous Machine with Winding Connection Change Method for High Efficiency EV Traction. In Proceedings of the 2021 IEEE Vehicle Power and Propulsion Conference (VPPC), Gijon, Spain, 25–28 October 2021; pp. 1–6.
33. Berringer, K.; Marvin, J.; Perruchoud, P. Semiconductor power losses in AC inverters. In Proceedings of the Industry Applications Conference, 1995. Thirtieth IAS Annual Meeting, IAS'95, Orlando, FL, USA, 8–12 October 1995; pp. 882–888.
34. Infineon Technologies AG. *HybridPACK Drive Module*, Rev. 3.0; Infineon Technologies AG: Hong Kong, China, 2019.
35. Markel, T.; Brooker, A.; Hendricks, T.; Johnson, V.; Kelly, K.; Kramer, B.; O'Keefe, M.; Sprik, S.; Wipke, K. ADVISOR: A systems analysis tool for advanced vehicle modeling. *J. Power Sources* **2002**, *110*, 255–266. [CrossRef]